Accuracy Analysis of Incrementally Formed Tunnel Shaped Parts

Accuracy analysis of incrementally formed tunnel shaped parts

Amar Kumar Behera[1] , Daniel Afonso[2], Adrian Murphy[1], Yan Jin[1], Ricardo Alves de Sousa[2]

[1] School of Mechanical and Aerospace Engineering, Queen's University Belfast, Stranmillis Road, Belfast BT9 5AH
[2]Department of Mechanical Engineering, University of Aveiro, Campus de Santiago, 3810-183 Aveiro, Portugal
{a.behera@qub.ac.uk, dan@ua.pt, a.murphy@qub.ac.uk, y.jin@qub.ac.uk, rsousa@ua.pt}

Abstract. Tunnel shaped parts with truncated pyramidal shapes were formed using Single Point Incremental Forming (SPIF) on a Stewart platform. The accuracy behavior of these parts was characterized by an error prediction response surface generated using Multivariate Adaptive Regression Splines (MARS). This response surface predicted over forming for low wall angle parts and under forming for higher wall angle parts. It is based on geometrical parameters associated with features on the part geometry and was used to compensate for inaccuracies in the part geometry. Feature detection was found to work well for tunnel shaped parts using similar thresholds as container shaped parts, while the maximum deviations were found to be lower at a wall angle of 60° compared to a part with wall angle 40°.

Keywords: tunnel shaped parts, single point incremental forming (SPIF), MARS, accuracy, sheet metal

1 Introduction

Single Point Incremental Forming (SPIF) is a flexible sheet metal forming process that enables dieless manufacture of 3D shapes. A cylindrical tool with a hemispherical ball end is usually used to deform a flat sheet in incremental steps, conforming to the part geometry. The process has been studied in great detail over the last 15 years, leading to detailed understanding of the deformation mechanics and process outcomes such as sheet thickness variations, formability and achievable accuracy [1]. Several process variants have been developed that include the use of laser support [2], electrical heating [3], two tools [4], part die [5], full die [5] etc.

Most studies in SPIF have focused on the use of fully constrained sheets, clamped on four sides, resulting in parts that have the configuration of a container. The disadvantage in such a configuration is the waste of material when forming parts that are eventually not meant to be containers and limitation in part dimensions. To overcome these limitations, the forming of tunnel shaped parts, as shown in Fig. 1 has been recently proposed by Afonso et al. [6] This involves the use of semi-constrained

sheets where only two sides are clamped. The result of this is a reduction in the formability, leading to a lower critical wall angle at failure. Furthermore, the deformation characteristics change leading to inaccuracies with different magnitudes and shape as compared to fully constrained blanks.

The objective of the current study was to investigate the effect of semi-constraining on the achievable part accuracy. Pyramidal shapes with three different wall angles were formed and their accuracy behavior studied. The formed surfaces were compared to their nominal CAD models and the resulting data sets were used to train a regression model using Multivariate Adaptive Regression Splines (MARS) for individual planar features on the parts. This model was then used to compensate for the part accuracy, resulting in compensated STL files, which can be used for optimized toolpath generation for tunnel shaped parts.

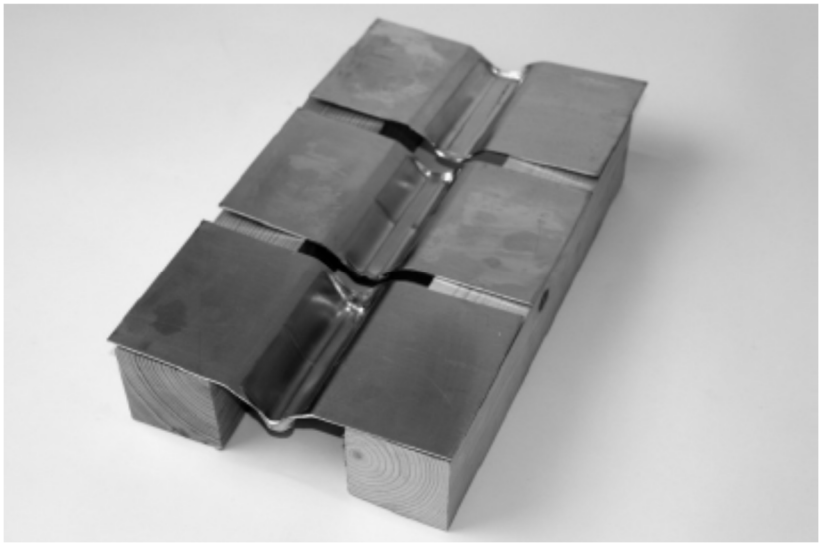

Fig. 1. Tunnel shaped parts formed using Single Point Incremental Forming (SPIF)

2 Methodology

The experimental and analysis campaign is described below. First, the experimental setup is discussed. Next, the toolpath generation procedure for forming the parts in these experiments is described. A feature based part geometry compensator that works on part geometries in stereolithographic (STL) file format was used within this research, which is covered next. Finally, the methodology for accuracy prediction using the data from the experiments and linking to the part geometry compensator is discussed.

2.1 Experimental setup

Experimental tests were performed on the SPIF-A setup at Aveiro [7]. This setup possesses 6 degrees-of-freedom for the tool and uses a parallel kinematics scheme on a Stewart platform as its backbone architecture. Parts were made from aluminium sheets, AA 1050-H111, with a sheet thickness of 2 mm. A 10mm spherical tip punch was used, with a 0.5 mm constant step down in the z-axis (corresponding to the spindle axis), with a feed rate of 1500mm/min, free spinning tool and using 10W40 oil as a lubricant. Truncated tunnel shaped pyramids with wall angles 20°, 40° and 60° were formed and analysed for their accuracy behavior.

2.2 Toolpath generation for tunnel shaped parts

The toolpath strategy uses alternating directions in each forming step, with the travel from one wall of the tunnel to the opposite made outside the part edge, as shown in Fig. 2. The toolpath programming was done using Powermill. The CAD model surface was extended by 5mm on each edge (to allow a side changing position outside the true part edge) and a constant Z strategy was applied. The direction of the even steps were then changed. The toolpath was then post-processed to a numeric G-code to be run on the SPIF-A machine.

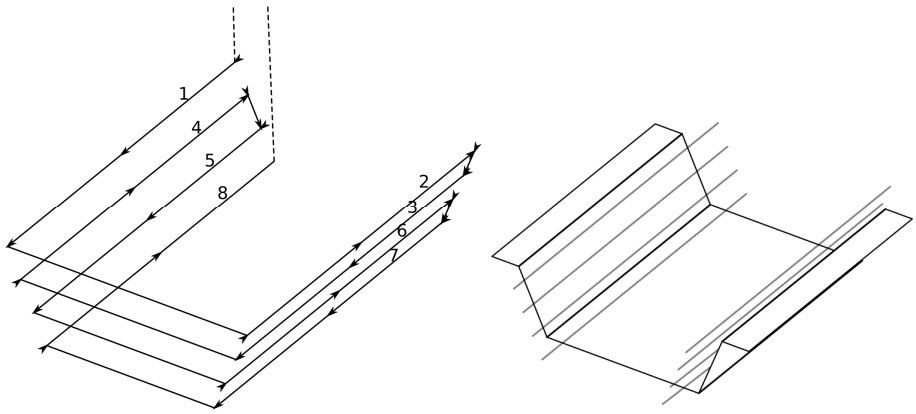

(a) (b)

Fig. 2. Toolpath strategy for tunnel shaped parts illustrating (a) movements of tool between passes 1-8 (b) length of tool movements on the part geometry

2.3 Feature detection on STL files

Past work on accuracy in SPIF has illustrated the strong correlation between geometrical features and the nature and magnitude of deviations in formed parts [8–10]. A taxonomy of 33 features based on geometry, curvature, orientation, location and process related attributes was defined by Behera et al. [11, 12]. These features can be detected within a Visual C# program, developed at KU Leuven, that takes in stereolithographic (STL) files as inputs, where the geometry of a part is described using triangles.

The feature detection process involves calculation of the principal curvatures and normal at each individual vertex in the STL model. This is done by following the steps outlined by Lefebvre et al. [13] The curvature tensor at a vertex v is calculated as:

$$\Lambda(v) = \frac{1}{|A|}\sum_{edges}\beta(e)\|e \cap A\|\frac{ee^T}{\|e\|^2} \quad (1)$$

where, |A| is the surface area of the spherical zone of influence of the tensor and *β(e)* is the signed angle between the normal vectors of the STL facets connected by the edge *e*. *β(e)* is positive for a concave surface and negative for a convex surface. The factor e ∩A gives the weight for the contribution by an individual edge. The normal at each vertex is estimated as the eigenvector of Λ(v) calculated by the eigenvalue of minimum magnitude. The remaining eigenvalues, k^{min} and k^{max} represent the minimum and maximum curvatures at the vertex *v*. Using these principal curvatures, four types of features can be classified as defined below:

Planar feature: $k^{min} = 0 \pm \varepsilon_p$ and $k^{max} = 0 \pm \varepsilon_p$, where ε_p is a small number that can be tuned for identifying planar features.

Ruled feature: $k^{min} = 0 \pm \varepsilon_r$ and $k^{max} = X$, where X is a positive non-zero variable. Another possible case is where $k^{min} = X$ and $k^{max} = 0 \pm \varepsilon_r$, where X is a negative non-zero variable. ε_r is a small number that can be tuned for identifying ruled features.

Freeform feature: $k^{min} = Y \pm \varepsilon_f$ and $k^{max} = X \pm \varepsilon_f$, where X and Y are non-zero variables such that $X \leq \rho_{\max}$ and $Y \geq \rho_{\min}$, where $\rho_{\max}$ and $\rho_{\min}$ are threshold values for distinguishing freeform and rib features. ε_f is a small number that can be tuned for identifying freeform features.

Rib feature: $k^{min} \leq \rho_{min}$ and/or $k^{max} \geq \rho_{max}$

2.4 Accuracy predictions using Multivariate Adaptive Regression Splines

In order to make reliable predictions of accuracy of sheet metal parts formed by SPIF, models can be developed using data from experimental parts. A common approach is to scan these parts with a laser scanner or touch probe, which generates a point cloud of high order (data sets of the order of 100, 000 – 500, 000 points). Once this cloud is generated, it can then be meshed to form a STL file and compared with the CAD model

corresponding to the design of the part (also commonly referred to as the nominal model), to generate a dataset of deviations for each individual point. This dataset can then be used to model the accuracy for a given feature as a function of key geometrical parameters on the feature. One technique for doing so that has been shown to effective for parts made by SPIF is the use of Multivariate Adaptive Regression Splines (MARS) [14]. MARS is a non-parametric regression technique that sifts through a data set and finds out the best possible relationship between the predictor variables and a response variable. A continuous response surface is generated with continuous first order derivative. Models typically take the form:

$$\hat{f}(x) = \sum_{n=1}^{N} c_n B_n(x) \tag{2}$$

The response variable is a weighted sum of basis functions $B_n(x)$, and the coefficients c_n are constants. The basis function $B_n(x)$ takes on one of three forms:

i) a constant,
ii) a hinge function of the type max(0, x – c) or max(0,c – x), where c is a constant and max(p, q) gives the maximum of the two real numbers p and q or
iii) a product of two or more hinge functions that models interactions between two or more variables.

The hinge functions have knots that are given by constants which are calculated by a forward pass step that initially over-fits the given data, and is followed by a backwards pruning operation which identifies terms that are to be retained in the model. MARS models provided in this paper were fitted in R, a statistical software suite developed as a GNU project, with functions associated with the 'Earth' library of R [15].

3 Results

In this section, detailed accuracy results from the three truncated tunnel shaped pyramid tests are presented first. Results for detection of features on such parts are covered next, followed by the MARS model for error prediction based on the accuracy data from these three tests. Finally, part compensation results are presented.

3.1 Accuracy analysis

By comparing the measured part geometries to the nominal CAD model in the software GOM Inspect, accuracy plots were obtained for the three truncated pyramids as shown in Fig. 3. The accuracy results were further analyzed by exporting the deviations for individual points and analyzing the same using a MATLAB code to yield a table of deviations, as shown in Table 1. The results indicate that the low wall angle part with a wall angle of 20° shows a significant amount of over forming, as indicated by a minimum deviation of -3.66 mm, while the under forming is highest for the part with the wall angle of 40°, where a maximum deviation of 5.47 mm is observed. The 60°

part shows an even distribution of under formed and over formed regions with a maximum deviation of 3.56 mm and a minimum deviation of -2.62 mm.

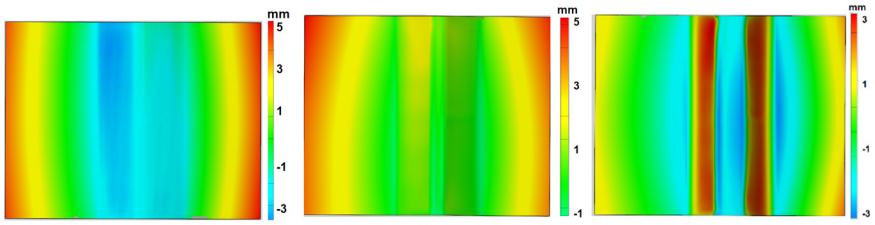

(a) (b) (c)

Fig. 3. Accuracy plots for parts with wall angles (a) 20°, (b) 40° and (c) 60°

Table 1. Accuracies of manufactured parts *(All dimensions are in mm)*

Wall angle	Average Positive Deviation	Average Negative Deviation	Maximum Deviation	Minimum Deviation	Average Deviation	Standard Deviation
20°	2.3298	-1.9974	5.2966	-3.6686	0.0541	2.4474
40°	1.8977	-0.3931	5.4758	-1.0077	1.6325	1.4430
60°	1.4554	-1.2095	3.5675	-2.6214	0.1573	1.5693

3.2 Feature detection results

Feature detection was carried out on the three STL files with a set of thresholds, as provided in Table 2. These thresholds have been generated after tuning them for tunnel shaped parts. The detection result for the 20° truncated pyramid is shown in Fig. 4. It was found that for shallow parts with low wall angles, the bottom horizontal plane may get detected as an edge occasionally. This is owing to only a small number of triangles available for feature detection and the presence of an edge when the ordinary non-horizontal planar (ONHP) feature meets the horizontal bottom planar (HBP) feature. It may be noted that the taxonomy adopted is the same as [11, 12].

Table 2. Feature detection thresholds

Threshold	Value
ε_p	$5*10^{-4}$
ε_r	10^{-5}
ε_f	10^{-5}
ρ_{min}	-0.01
ρ_{max}	0.01

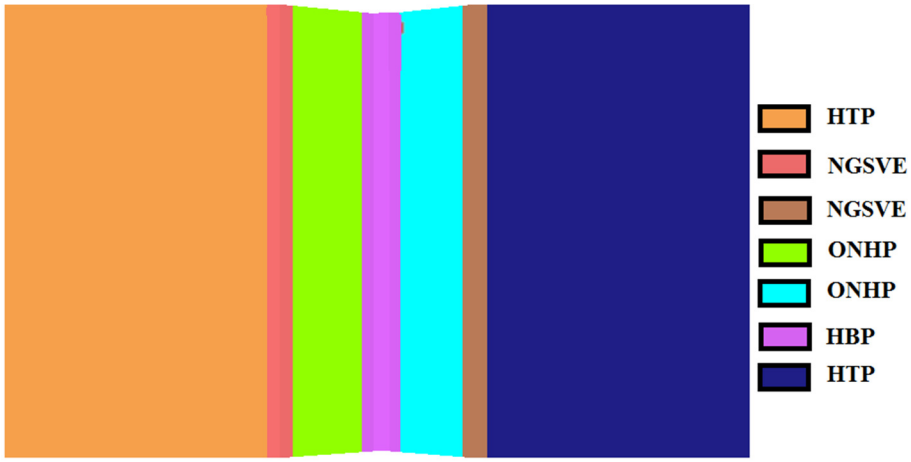

Fig. 4. Feature detection results on the 20 degree truncated pyramid (Nomenclature follows taxonomy defined in [11]; *HTP: Horizontal Top Planar, NGSVE: Negative General Semi-Vertical Edge, ONHP: Ordinary Non-Horizontal Planar, HBP: Horizontal Bottom Planar*)

3.3 Error correction (accuracy prediction) equation

The accuracy data from the three truncated pyramidal tests were used to train a MARS model. This yielded the following equation:

$$e = -0.58 + 0.57 * \max(0, 0.39 - d_b) + 0.49 * \max(0, d_b - 0.39) + 0.22 * \max(0,0.77 - d_o) - 3.4 * \max(0, d_o - 0.77) + 0.0085 * \max(103 - d_h) + 0.0028 * \max(0, d_h - 103) - 7.8 * \max(0,0.7-\propto) + 5.5 * \max(0, \propto -0.7) \quad (3)$$

Here, d_b is the normalized distance from the point on the STL file to the edge of the feature in the tool movement direction, d_o is the normalized distance from the point to the bottom of the feature, d_h is the total horizontal length of the feature at the vertex and $\propto$ is the wall angle at the vertex in radians.

3.4 Part compensation

Using the model generated in (3), vertices in the STL model of the part were translated normal to the part geometry, following the procedure outlined in [8], using a compensation factor of +1. The result of the compensation for a part with wall angle 40° is illustrated in Fig. 5. This compensated part geometry has been sent to the University of Aveiro for manufacture. It was noted that the model in (3) predicts over forming for low wall angle parts such as the one in the experimental test cases with wall angle of 20°, while it predicts under forming for higher wall angle parts such as the test cases with wall angles 40° and 60°.

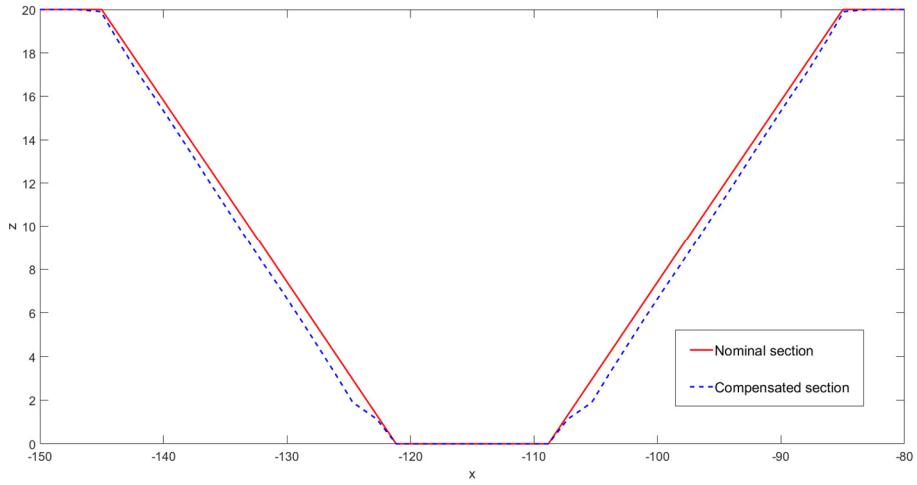

Fig. 5. Sectional view midway through the part at y = 70 mm from the part edge for a part with a length of 140 mm showing nominal and compensated sections

4 Discussion

The accuracy behavior at low wall angles for tunnel shaped pyramidal parts made by SPIF is similar to the behavior observed for fully constrained parts, both showing significant over forming. However, as the wall angle in increased, there appears to be divergence between the accuracy profiles. For fully constrained parts, the under forming at 60° is usually higher than at 40°. For tunnel shaped parts, the opposite behavior was observed in this set of experiments. This suggests that the material flow under deformation could be different for tunnel shaped parts compared to fully constrained parts. However, this will need further validation with additional experimentation such as the use of digital image correlation (DIC). It is also noteworthy that in prior work, Afonso et al. [6] indicated that the accuracy is lower in tunnel shaped parts when tool plunge movements are used in the center of the part, lateral movements of the tunnel bottom while forming due to absence of rigidity and damage at the edge of the parts. These factors influence the accuracy magnitudes that have been reported in this work.

Feature detection for truncated pyramidal parts using an established strategy as shown earlier by Behera et al. [8, 12] worked well here. The detection thresholds also did not change much compared to fully constrained parts. No additional changes to algorithms were necessary. Some cases showed the horizontal bottom being detected as an edge due to the low volume of triangulation for smaller parts and also the transition from a plane to another inducing a positive horizontal edge.

The MARS model shown in Equation (3) was able to predict and compensate the accuracy behavior of tunnel shaped parts. The efficacy of these predictions in improving the accuracy of parts will need further experiments. The optimized compensation factor for tunnel shaped parts could be different from fully constrained parts, as the results on accuracy at high wall angles indicate that deformation mechanisms seem to be different upon removal of constraints.

5 Conclusions

The analysis of accuracy behavior of truncated pyramids formed as tunnels using SPIF indicates continuation of some patterns observed for fully constrained parts such as over forming at low wall angles and introduction of potentially new phenomena such as higher accuracies at high wall angles compared to moderate wall angles. It is feasible to detect features on STL models of tunnel shaped parts, similar to fully constrained parts, with none or minimal changes to thresholds used for fully constrained parts. Compensation for part accuracy was carried out using a regression model using MARS and generated from the experiments performed in this study. Three distance parameters and the wall angle of the part were found to be the key predictor variables in the MARS model.

Further work shall involve looking into the effect of different compensation factors in improving the accuracy of formed parts. The effect of interaction between features can be studied by forming two slope pyramids and cones, to understand the deformation mechanisms better, make good predictions and form complex parts. The effect of material properties and sheet thickness on accuracy profiles can be studied using digital image correlation leading to better predictions using generic error correction functions.

References

1. Behera, A.K., de Sousa, R.A., Ingarao, G., Oleksik, V.: Single point incremental forming: An assessment of the progress and technology trends from 2005 to 2015. J. Manuf. Process. 27, 37–62 (2017).
2. Duflou, J.R., Callebaut, B., Verbert, J., De Baerdemaeker, H.: Laser assisted incremental forming: Formability and accuracy improvement. Cirp Ann. Technol. 56, 273–276 (2007).
3. Fan, G.Q., Gao, L., Hussain, G., Wu, Z.L.: Electric hot incremental forming: A novel technique. Int. J. Mach. Tools Manuf. 48, 1688–1692 (2008).
4. Malhotra, R., Cao, J., Ren, F., Kiridena, V., Xia, Z.C., Reddy, N. V: Improvement of Geometric Accuracy in Incremental Forming by Using a Squeezing Toolpath Strategy With Two Forming Tools. J. Manuf. Sci. Eng. Asme. 133, (2011).
5. Jeswiet, J., Micari, F., Hirt, G., Bramley, A., Duflou, J., Allwood, J.: Asymmetric single point incremental forming of sheet metal. Cirp Ann. Technol. 54, 623–649 (2005).
6. Afonso, D., Sousa, R.A. de, Torcato, R.: Incremental Forming of Tunnel Type Parts. Procedia Eng. 183, 137–142 (2017).

7. de Sousa, R.J.A., Ferreira, J.A.F., de Farias, J.B.S., Torrão, J.N.D., Afonso, D.G., Martins, M.: SPIF-A: on the development of a new concept of incremental forming machine. Struct. Eng. Mech. 49, 645–660 (2014).
8. Behera, A.K., Verbert, J., Lauwers, B., Duflou, J.R.: Tool path compensation strategies for single point incremental sheet forming using multivariate adaptive regression splines. Comput. Des. 45, 575–590 (2013).
9. Behera, A.K., Lauwers, B., Duflou, J.R.: An Integrated Approach to Accurate Part Manufacture in Single Point Incremental Forming using Feature Based Graph Topology. Mater. Form. - Esaform 2012, Pts 1 2. 504–506, 869–876 (2012).
10. Verbert, J., Duflou, J.R., Lauwers, B.: Feature based approach for increasing the accuracy of the SPIF process. Sheet Met. 2007. 344, 527–534 (2007).
11. Behera, A.K., Lauwers, B., Duflou, J.R.: Advanced feature detection algorithms for incrementally formed sheet metal parts. Trans. Nonferrous Met. Soc. China. 22, S315–S322 (2012).
12. Behera, A.K., Duflou, J., Lauwers, B.: Shape Feature Taxonomy Development for Toolpath Optimisation in Incremental Sheet Forming. PhD Thesis. KU Leuven. (2013).
13. Lefebvre, P., Lauwers, B.: Multi-axis machining operation evaluation for complex shaped part features. In: Proceedings of the 4th CIRP International Seminar on Intelligent Computation in Manufacturing Engineering. pp. 345–350 (2004).
14. Behera, A.K., Gu, J., Lauwers, B., Duflou, J.R.: Influence of Material Properties on Accuracy Response Surfaces in Single Point Incremental Forming. Mater. Form. - Esaform 2012, Pts 1-2. 504–506, 919–924 (2012).
15. Milborrow, S.: earth: Multivariate Adaptive Regression Splines, https://cran.r-project.org/web/packages/earth/index.html. Last accessed 16th May, 2018